Cancer Treatment and Research Communications 21 (2019) 100157

Contents lists available at ScienceDirect

Cancer Treatment and Research Communications

journal homepage: www.elsevier.com/locate/ctarc

Evaluation of cytotoxic activity of docetaxel loaded gold nanoparticles for lung cancer drug delivery

S. Thambiraj[a], S. Shruthi[b], R. Vijayalakshmi[b], D. Ravi Shankaran[a,*]

[a] Nano-Bio Materials and Sensors Laboratory, National Centre for Nanoscience and Nanotechnology, University of Madras, Guindy Campus, Chennai 600025, India
[b] Department of Preventive Oncology, Cancer Institute (WIA), Adyar, Chennai 600020, India

ARTICLE INFO

Keywords:
Gold nanoparticles
Cytotoxicity
Lung cancer
Docetaxel
Targeted drug delivery
HR-TEM

ABSTRACT

The effective use of the gold nanoparticle (AuNPs) conjugated drugs for targeted drug delivery applications is one of the most promising research areas in the field of cancer. Herein, we aimed to establish a nano drug conjugated with docetaxel as a possible therapy option. Gold nanoparticles were synthesized by chemical reduction method. This is followed by the conjugation with an anticancer drug, docetaxel (Dtx) by a non-covalent method and folic acid (FA) was conjugated by a covalent method. The physicochemical characteristics of the synthesized AuNPs, Dtx and FA were studied by various analytical techniques such as UV–vis spectroscopy (UV–vis), Fourier transform infrared spectroscopy (FTIR), X-ray diffraction (XRD), Raman spectroscopy, X-ray photoelectron spectroscopy (XPS), field emission scanning electron microscope (FE-SEM) high-resolution transmission electron microscope (HR-TEM) and energy dispersive X-ray spectroscopy (EDS). The surface morphology and microstructure of the synthesized AuNPs and gold conjugates (AuNPs-Dtx-FA) were examined by FESEM and HR-TEM. The average size of the spherical shaped AuNPs was observed in the range of 5–18 nm. XPS and EDS spectra were examined the oxidation state and chemical composition of the synthesized nanoparticles. The cytotoxicity of the synthesized AuNPs nano-conjugates was evaluated by in-vitro studies against lung cancer cell line (H520). The chemical reduction method followed here in the development of AuNPs is a simple and one-step process, which exhibits the excellent binding specificity, biocompatibility and feasible for the large scale up process of the AuNPs.

1. Introduction

The use of functional nanomaterials as carriers for high-performance drug delivery application is an area of expanding interest around the world. Among the various nanomaterials, gold nanoparticles (AuNPs) are found to be an excellent candidate for targeted drug delivery due to their characteristic features which include unique physiochemical properties which allow for easy surface modifications, facile conjugation with biomolecules, relatively high biocompatibility and low-toxicity [1–4]. Based on their unique properties, the gold based nanoconjugates have been widely used in myriad applications including biosensor, bioimaging, photothermal therapy and targeted drug delivery [5–8]. The size controlled AuNPs can be synthesized by various methods like physical, chemical and biological methods. Among them, the chemical reduction method has been widely used for the synthesis of AuNPs due to its low-toxicity, highly stable, and less time consumption [9–11]. The chemical reduction method plays a vital role in the production of functional nanomaterials [12].

Docetaxel (Dtx), an anticancer drug, belongs to the family of taxanes, diterpenes produced by plants of the genus Taxus [13]. Like paclitaxel, Dtx is a semi-synthetic material that irreversibly binds to β-actin, and consequently alters the microtubule polymerization and disrupts cell mitosis and trigger apoptosis [14]. Dtx based treatment is an option in the patients for hormone-refractory of lung cancer and it has been shown to increase the survival of patients [15]. Dtx treatment though is associated with several toxicities, based mostly on the dose and duration of the therapy [16]. A major drawback of Dtx treatment lies in its poor hydrophilicity [17].

Folic acid (FA) is an emerging ligand for targeting cells membrane receptor on the range of cell type and retains a high affinity for its receptor [18]. Therefore, FA and AuNPs based conjugates have significantly enhanced delivery to folate receptor (FR) in the positive tumor cells because the FR are frequently overexpressed in a wide variety of tumor cells but highly restricted in most normal tissues [19]. FA or its conjugates are transporting the surface of cancer cells via endocytosis through the folate receptor at the pH range of 5.0–5.5

* Corresponding author.
E-mail addresses: dravishankaran@hotmail.com, dravishankaran@unom.ac.in (D. Ravi Shankaran).

https://doi.org/10.1016/j.ctarc.2019.100157

[20,21]. Moreover, the high specific area and spherical morphology of gold based nanoconjugates can be used as an effective nanocarrier in targeted drug delivery applications [11].

Lung cancer (lung carcinoma) is the most common malignancy in men and the second most common in women. Chemotherapy while a common treatment option is limited by low specificity and high general toxicity [22,23]. Owing to its limitations, the combination of controlled release and targeted drug delivery will exhibit a more effective approach [24]. Thus, the development of nanoconjugates that fulfill these criteria is expected to aid in better cancer therapy [25]. Recently, AuNPs have been utilized for anticancer therapy for several types of cancers such as lung cancer cell line (A549, and H1299) [25,26], prostate cancer cell lines (PC3) [27] and Du145 cell line [28], breast cancer cell lines (MCF 7) [29] and liver cancer cell line (HepG2) [24].

In the present work, we aimed to investigate a simple and efficient method for the synthesis of AuNPs by chemical reduction method. The synthesized AuNPs were conjugated with docetaxel as the chemotherapeutic drug and FA by non-covalent and covalent method, respectively. The surface morphology features and size distribution of the AuNPs based nanoconjugates were studied by HR-TEM and FE- SEM. The oxidation state and elemental composition of the synthesized AuNPs based nanoconjugates were studied using XPS and EDS analysis. The cytotoxicity of these AuNPs nanoconjugates was assessed by in-vitro studies against lung cancer cell line (H520) at different concentrations and time intervals.

2. Experimental section

2.1. Materials

Gold (III) chloride trihydrate ($HAuCl_4{\bullet}3H_2O$, M.W. 393.83 g/mol), Docetaxel (DTX) ($C_{43}H_{53}NO_{14}$, M.W. 807.879 g/mol), Folic acid (FA) ($C_{19}H_{19}N_7O_6$, MW. 441.40 g/mol) and 10% Fatal bovine serum (FBS) were procured from Sigma Aldrich Chemicals, USA. Trisodium citrate ($Na_3C_6H_5O_7$, MW. 258.06 g/mol), N, N-Dimethyl sulfoxide (DMSO) (C_2H_6OS) were purchased from Merck chemicals. Ethanol (99.9%) was received from Changshu Hongsheng Fine Chemical Co., Ltd, China. Pre-Mix WST was procured from Takara Scientific. RPMI 1640 medium was purchased from Himedia chemicals, Mumbai, India. Human Lung cancer cell line (H520) was received from National Centre for Cell Science (NCCS), Pune, India. All the chemicals were used without any purification and millipore water was used throughout the work.

2.2. Methods

2.2.1. Synthesis of gold nanoparticles

A modified procedure has been used for the synthesis of gold nanoparticles from Gold (III) chloride trihydrate using trisodium citrate as a reducing agent, by the chemical reduction method [9–11].

Briefly, 5 mL of 1 (wt%) of trisodium citrate in aqueous medium was added dropwise to a 200 mL aliquot of 1 mM $HAuCl_4{\bullet}3H_2O$ boiling with stirring the solution under reflux. After adding the reducing agent, the reaction mixtures color changed from golden yellow to colorless. This reaction was continued until the solution turned to wine red. This color change appeared within 3 min due to the reduction of Au^{III} to Au^0 and the reaction was completed within 5 min. The obtained colloidal suspension was allowed to cool at room temperature. After the completion of the reaction, the loosely bounded citrate ions were removed by centrifuge at 5000 rpm for 30 min and the obtained AuNPs the solution was stored at 4 °C.

2.2.2. Preparation of gold based nanoconjugates

In order to prepare the gold based conjugate, 5 mL of 1 mM of Dtx was dissolved in ethanol and sonicated for 15 min. This aliquot solution was added to the synthesized AuNPs in a 50 mL glass beaker with constant stirring, for 3 h. Followed by, the obtained Dtx loaded AuNPs solution was sonicated for 20 min in an ice bath. Thereafter, 3 mL of 1 mM of FA was dissolved in DMSO under constant stirring for 1 h at room temperature. The prepared solution was added into Dtx loaded AuNPs solution and stirred for 4 h at room temperature. After this solution was sonicated for 30 min, it was centrifuged at 5000 rpm for 30 min. The obtained solution was stored at 4 °C in order to prevent aggregation.

2.3. Characterization studies

2.3.1. High-Resolution scanning electron microscope

The morphology and microstructure of the synthesized AuNPs were examined by high-resolution transmission electron microscope (HR-TEM) (JEOL-2100-JEM). 0.5 μL of AuNPs conjugate solution was diluted with Millipore water and sonicated for 10 min. A small drop of the conjugate was coated over a carbon coated copper grid and allowed to dry at ambient temperature. The dried samples were fixed on the sample holder and analyzed at 200 kV an acceleration voltage. The size distribution of the obtained conjugates was measured by image J (version 1.41 h) and origin pro-8 software. The elemental compositions of AuNPs/DTX/FA were measured by energy dispersive X-ray spectroscopy (EDS).

2.3.2. Field emission scanning electron microscope

The surface morphology of the synthesized AuNPs based conjugates was analyzed by field emission scanning electron microscope (FE-SEM) Hitachi-S-34000N (Japan) instrument. For sample preparation, 0.5 μl of AuNPs based conjugates were diluted with Millipore water and sonicated for 15 min. A small drop of the sonicated solution was coated over a cleaned aluminum substrate and the substrate was dried at room temperature. The dried samples were pasted over double sided carbon tape. The pasted samples were then sputter-coated with gold and platinum (60:40) for 25 s at 30 mA current and 0.4 mb pressure. These samples were then analyzed at an accelerating voltage of 20 kV.

2.3.3. X-ray diffraction

Crystallinity and phase purity of the obtained AuNPs/DTX/FA was studied by XRD analysis. XRD pattern was recorded on Bruker (D8 advance PXRD) equipment using a scanning rate of 2 s/step and (Johansson monochromator) to produce pure Cu Kα ($\lambda = 1.5406$ Å) radiation as a target with a voltage of 40 kV and current 30 mA. For sample preparation, a small amount of obtained solution was sonicated for 5 min and coated over the freshly prepared glass substrate. The sample coated glass substrate was dried at room temperature. The coated samples were scanned from 5° to 90° (2θ) degrees.

2.3.4. X-ray photoelectron spectroscopy

The oxidation state and elemental composition of the obtained samples were examined by X-ray photoelectron spectroscopy (XPS). XPS spectra were performed using an Omicron Nanotechnology, ESCA-14 (Germany) photoelectron spectrometer instrument. Al K-Alpha X-ray source of monochromatic in the “hybrid” mode of a nominal photoelectron was operated at 120 W (15 kV, 20 mA). For sample preparation, a small drop of 0.5 μl of AuNPs based conjugate solution was coated over the freshly prepared aluminum substrate and dried at 60 °C for 3 h. The dried samples were fixed with XPS sample holder and measurements were taken on three replicates for each sample. Data analysis was done using the vision processing data reduction software.

2.3.5. Raman spectroscopy

Raman spectra were collected on a Nano Photon-Raman spectrometer with laser excitation (532 and 785 nm). The data acquisition time was 30 s and the peak intensities of the samples were normalized to those of a glass plate at 520 cm^{-1}. The spectra were obtained in the range of $400-2500$ cm^{-1} with three accumulations, 10 s exposure times and spectral resolution of 16 cm^{-1}. For sample preparation, 1 mL

of the obtained solution was sonicated for 5 min and coated over a freshly prepared glass substrate. The sample coated glass substrate was dried at room temperature. The coated samples were examined with an excitation wavelength of 532 nm.

2.3.6. Fourier transform infrared spectroscopy

The surface functional groups of AuNPs based conjugates were determined by Fourier transform infrared spectroscopy (FT–IR) (Thermo scientific & co., ID 3, USA). The AuNPs based conjugate solution was diluted with Millipore water and analyzed under attenuated total reflection (ATR) mode. The samples were analyzed in the transmission mode with a spectral range from 400–4000 cm^{-1}, a spectral resolution of 4 cm^{-1} and a scanning speed of 20 mm/s at room temperature.

2.3.7. UV–vis spectroscopy

Optical properties of the synthesized gold based conjugates were examined by UV–vis absorption spectroscopy (UV–vis) (Agilent diodaris spectrophotometer, Cary-8453, India). The spectra were recorded on double beam standard quartz cuvettes with the spectral range of 200–800 nm at room temperature. 5 µl of AuNPs based nanoconjugates were diluted with Millipore water and sonicated for 5 min and analyzed by the spectrophotometer.

2.3.8. MTT assay

100 µL of H520 cells were seeded in 96 well plates (Corning, USA) at the density of 3000 cells per well and incubated at 37 °C for 24 h in a CO_2 incubator for 24 h before the experiment. The cells were incubated with free AuNPs, Dtx, FA and AuNPs based nanoconjugates at a concentration ranging from 10 to 100 µM and 5 to 200 pM in the case of FA and analysed at 24, 48 and 72 h, time points. At the time these intervals, the medium was removed and the plate was washed with PBS two times. The cells were then incubated for a maximum of 4 h in WST. The absorption was measured at 560 nm using ELISA (Enzyme-linked immunosorbent assay) microplate reader (Robonik). The cell viability was calculated by the following equation:

$$\text{Cellviability}(\%) = (\text{Abssample}/\text{Abscontrol})\text{x}100.$$

where, Abs sample represents the number of absorbance for the treated cells and Abs control represents the number of absorbance for control cells in culture medium only. All the experiments were carried out three times.

2.3.9. Statistical analysis

The cell, culture data were expressed as a mean of three experiments ± standard deviation (SD). The significance of AuNPs, Dtx, FA, and nanoformulations data performed by one-way analysis of variance (ANOVA), followed by post hoc test for comparison with group A (SPSS 16.0 software (SPSS Inc. Chicago, IL, USA)). The significance level of 95% is acceptable value ($p < 0.05$) [30].

3. Results and discussion

AuNPs were synthesized by the chemical reduction method of trisodium citrate which acts as a capping and as well as a stabilization agent. Nanoconjugates of the AuNPs have been prepared by functionalization with docetaxel (Dtx) and folic acid (FA). The influence of the reaction condition on the morphology of the AuNPs based nanoconjugates and their characteristics have been evaluated with respect to the concentration of the reactant, temperature, reaction time and pH. When reducing the temperature during citrate reduction, the size, shape and quality of the particles were drastically affected and the final product appeared to be of a larger size and with irregular morphology. Fig. 1 depicts the scheme for the synthesis of AuNPs based nanoconjugates by the chemical reduction method.

3.1. Surface morphology of gold based nanoconjugates

The morphology and microstructure of the synthesized AuNPs based nanoconjugates were studied by HR-TEM and FE-SEM analysis. A typical HR-TEM measurement of the synthesized AuNPs is shown in Fig. 2. Fig. 2(a) depicts the higher magnification (2 nm) image of AuNPs which shows the clear and uniform lattice fringes confirming that the particles are spherical in shape with a high degree of crystallinity. Fig. 2 (b and c) shows the AuNPs at various magnifications (5 and 10 nm). The size of AuNPs has been determined by measuring the diameter of particles on TEM micrographs. Fig. 2(d) shows the low magnification image of AuNPs (100 nm) and the particles are in the mono-dispersion state due to the negatively charged layer of citrate ions, which repel each other. The average diameter of the obtained AuNPs was found to be 18 nm (Inserted the histogram on Fig. 2(d)) with very few particles of higher and lower size distribution. Fig. 2(e) depicts the selected area electron diffraction (SAED) pattern to AuNPs which shows higher crystallinity. The crystal lattice spacing distances of AuNPs is about 4.0786 Å and these lattice are accordance with the (200), (311) diffraction planes of gold (Joint Committee on Powder Diffraction Standards file No. 04-0784). Thus, the results indicate that the gold particles are arranged in a face centered cubic crystals system with $\lambda = 1.5406$ Å. The elemental compositions of the synthesized AuNPs were examined by EDS analysis. Fig. 2(f) depicts the EDS spectrum of synthesized AuNPs which indicates the 60.44 wt% of gold is present in the sample. The occurrence of copper 39.56 wt% is present in the spectrum due to the presence of the TEM grid was appeared in the spectrum. This result suggests that the synthesized AuNPs are highly pure and have good crystallinity.

FESEM micrograph of the synthesized AuNPs and AuNPs based conjugates are shown in Fig. 3. Fig. 3(a) depicts the FE-SEM images of AuNPs which shows the particles are spherical in shape with a uniform distribution on the aluminum substrate. The average size of the AuNPs was found to be 20 nm. Fig. 3(b) shows the low magnification image of docetaxel and it can be observed that the particles are randomly dispersed on the surface of the substrate. These particles are present in the form of core-shell like particles and were observed to have an average size of 25 nm. Fig. 3(c) indicates the low magnification images of folic acid which shows that these particles are spherical in shape with an average diameter of 440 nm. Fig. 3(d) shows the FE-SEM image of AuNPs based conjugates and the particles are spherical in shape with a smooth surface, without any aggregation. Fig. 3 (e and f) shows the EDS spectra of the drug molecule and AuNPs based conjugates.

3.2. Crystallinity of the AuNPs based conjugates

Crystalline nature of the synthesized AuNPs was determined by XRD analysis. Fig. 4(a) depicts the XRD pattern of citrate capped AuNPs. The Bragg reflection indicates the synthesized AuNPs possess the face centered cubic crystal structure in nature. The XRD pattern exhibits the diffraction band at (2θ) 38.21°, 40.36°, 44.39°, 64.76° and 77.76° which corresponds to the (111), (200), (220) and (311) crystal planes, respectively [31]. These diffraction peaks indicate that these AuNPs are composed of pure crystalline gold is confirmed by JCPDS (Joint Committee on Powder Diffraction Standards file No. 04-0784). In the XRD pattern, the most intense Bragg reflection lattice planes appear at (111) and (200) of planar surface are 100% and 19% respectively, whereas, the Bragg reflection corresponding to the (220) and (311) planes with the lattice spacing planes of 1.44 and 1.23 A°. These planes indicate the {111} facets were indicating the crystalline nature of AuNPs.

Fig. 4 (b and c) indicates the XRD spectra of docetaxel and folic acid, respectively. The most intense band appears at 6°, 9°, 13°, and 21° of Dtx which shows the highly crystalline in orthorhombic in nature of Dtx (Fig. 4b) [32]. Fig. 4(c) shows indicates the sharper band at 10.4°, 20.2°, and 22.6° corresponds to the (101), (202) and (002) crystal planes of the FA, respectively [33]. Fig. 4(d) shows the XRD spectrum of

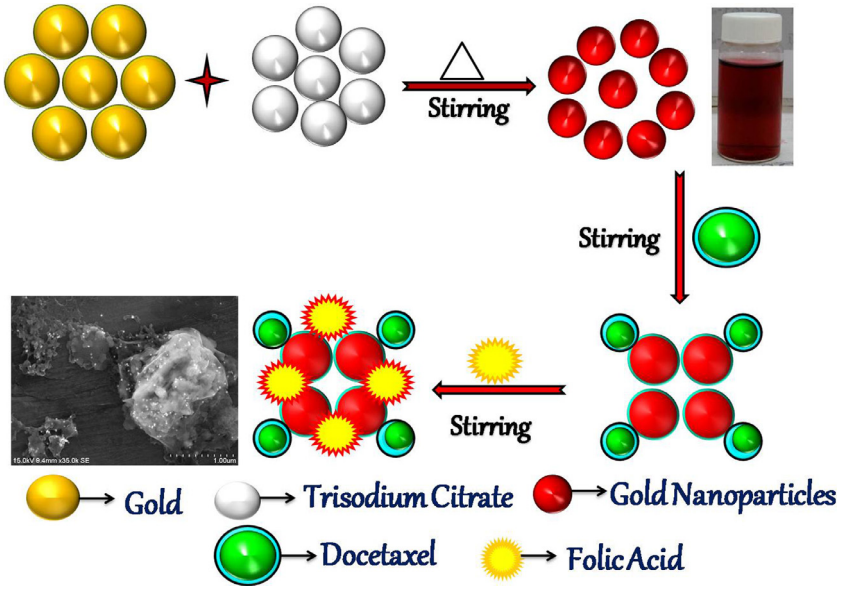

Fig. 1. Schematic representation of the synthesis of AuNPs based conjugates.

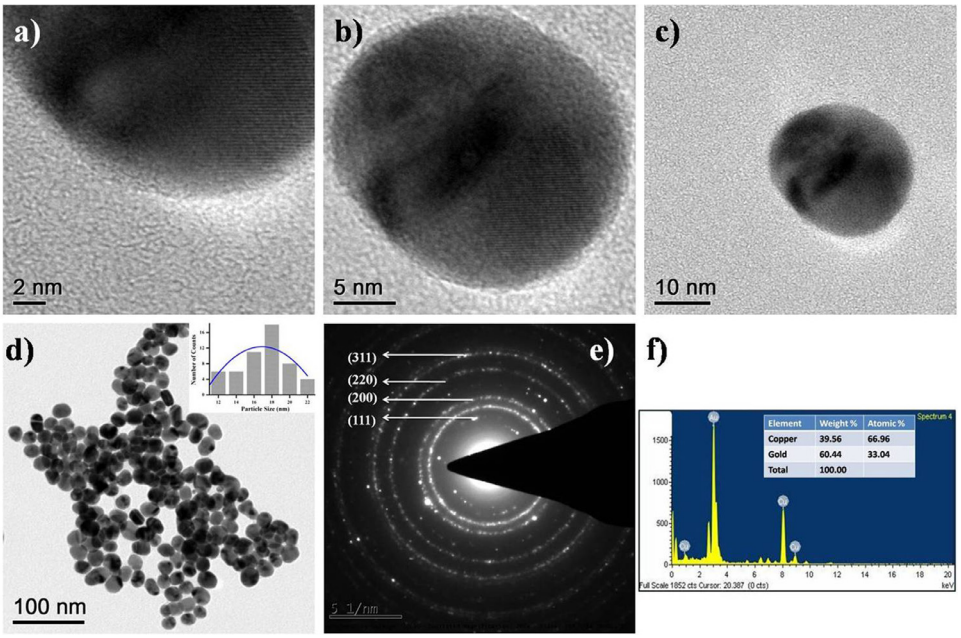

Fig. 2. HR-TEM images of citrate capped AuNPs. (a) HR-TEM image at 2 nm magnification particle shows the uniform lattice fringes, (b & c) Spherical shaped AuNPs at 5 and 10 nm magnifications, (d) TEM images of AuNPs and inset the histogram of the AuNPs. The average size is 18 nm (e) SAED pattern of the AuNPs and (f) EDS spectrum of AuNPs.

gold based conjugates of AuNPs/DTX/FA was observed at 2θ values of 6°, 13°, 22.6°, 26.2°, 38.21°, 44.39° and 77.76°. These bands indicate the gold based conjugates possess good crystallinity.

3.3. Structural analysis of gold based nanoconjugates

The oxidation state and elemental composition of the synthesized gold based nanoconjugates (AuNPs/Dtx/FA) were determined by X-ray photoelectron spectroscopy (Fig. 5). Fig. 5(a) shows the survey spectrum of AuNPs/ Dtx/FA, which shows the synthesized gold based nanoconjugates is high purity. The high-resolution spectrum of the AuNPs based nanoconjugates was observed the core levels of Au $4f_{7/2}$ and Au $4f_{5/2}$ spin orbital and the peak positioned at 85.3 eV and 88.9 eV, respectively (Fig. 5(b)) [34]. These values were compared to the respective core levels of bulk Au crystals. Moreover, the obtained peaks of Au $4f_{7/2}$ and Au $4f_{5/2}$ showing a narrow width revealed that only a single element of gold was present in the system. This result indicates that the gold was present in the metallic form of Au^0 and thus rendering the AuNPs highly stable. Fig. 5(c) depicts the high-resolution image of carbon (C1s) was observed the two peaks at 287.27 eV and 290.64 eV corresponds to the (C—C or C—H)/(C—O) (O—C—O) formations [35]. The binding energy of the nitrogen (N1s) (Fig. 5(d)) exhibited only one peak at 403.52 eV, which can be associated with the nitrogen atom present in the form of C═N/N—H [36]. Fig. 5(e) shows the high-resolution spectrum of oxygen (O1s) exhibited peaks at 534.38 eV which corresponds to the O—C—O/C═O [37]. These spectra clearly indicate that the synthesized AuNPs based nanoconjugates possess highly pure. Based on these results, we can also suggest that the synthesized nanoconjugates are pure, reaffirming with previous results.

Raman spectroscopy is used to identify the surface vibration and rotational frequency of the surface particles and also to observe the structural fingerprints of the particles. Fig. 5(f) shows the Confocal Raman spectra of the gold based conjugates. Fig. 5(f) (a) depicting the Raman spectra of the synthesized citrate capped AuNPs, we observed

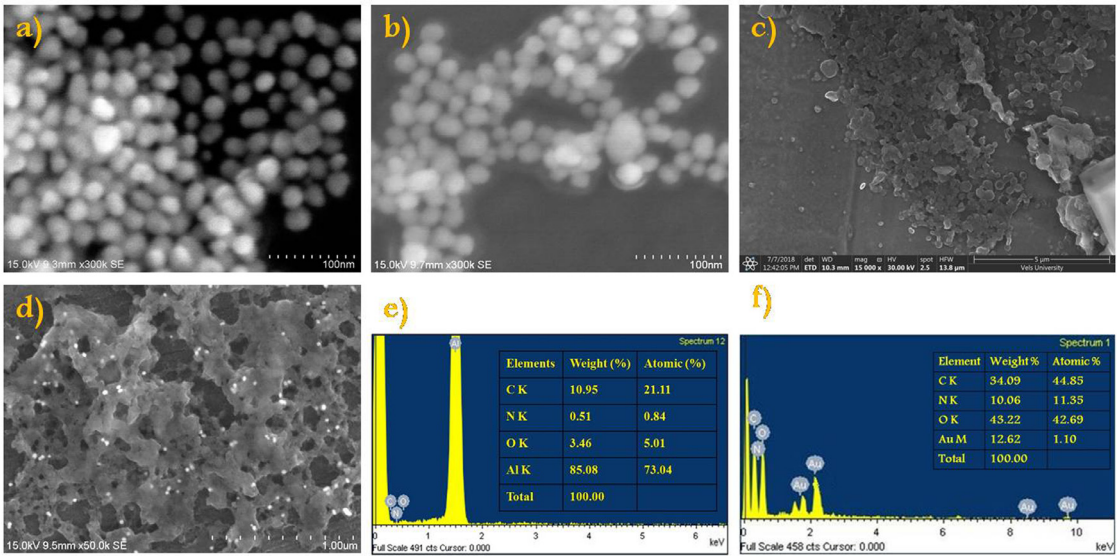

Fig. 3. FE-SEM images of AuNPs based nanoconjugates. (a) Spherical shaped AuNPs, (b) Dtx, (c) FA, (d) AuNPs/Dtx/FA nanoconjugates, (e and f), EDS spectrum of Dtx and AuNPs/PEG/Dtx/FA nanoconjugates, respectively.

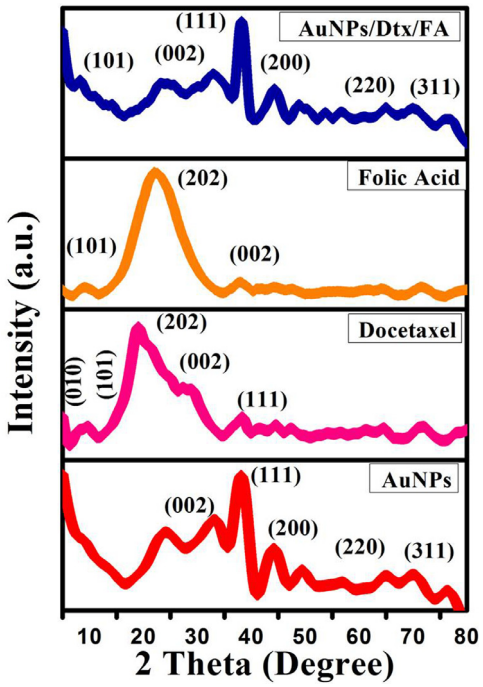

Fig. 4. XRD spectra of AuNPs based nanoconjugates. (a) AuNPs, (b) Dtx, (c) FA and (d) AuNPs/Dtx/FA conjugate.

peaks at 269 cm^{-1}, 1232 cm^{-1}, 1373 cm^{-1} and 1596 cm^{-1}corresponding to the Au^0 and carbon strongly observed on the surface [38]. Fig. 5(f) (b) shows the Raman spectra of the Dtx, which we observed had peaks at 820 $cm-^{1}$ (aromatic stretching vibration of C═C), 1220 cm^{-1} (C—H), 1373 cm^{-1}(C═C) and 1630 cm^{-1} (aromatic stretching vibration of C═O, carbonyl groups) [39]. Fig. 5(f) (c) shows the Raman spectra of FA which shows the strongest peaks at 689, 920, 1260, 1376 and 1590 cm^{-1}, which corresponds to the asymmetric vibration of the C═N, C—H rocking vibration of P-amino benzoic acid, rocking vibration of C═N, C═C asymmetric stretching vibration and aromatic stretching vibration of C═O carbonyl groups, respectively [40].

Fig. 6(d) depicts that the Confocal Raman spectra of AuNPs based conjugates contain a very strong peak at 269 cm^{-1} due to vibrations between Au^0 and C, reaffirming the SERS spectra document at AuNPs surfaces. Peaks at 857, 1293, 1378 and 1596 cm^{-1} were also observed, which documents the vibrations displayed by DTX and FA. The strong vibration peaks at 269 cm^{-1} and 1378 cm^{-1} correspond to the Au^0 and carbon particles. These vibration peaks indicate the structural fingerprints of the obtained AuNPs based conjugates are highly pure.

Surface functional groups of the synthesized AuNPs based nanoconjugates were studied by FT–IR spectroscopy (Fig. 6). Fig. 6 (a) (a) shows the FT–IR spectrum of AuNPs and the major peak was observed at 3289 cm^{-1}, which corresponds to the OH stretching vibration of the carboxyl group. The band at 2929 cm^{-1} corresponds to the C—H stretching vibration of alkanes. The strongest peak at 1704 cm^{-1} is attributed to C═O stretching vibration of amides. The weak band at 1365 cm^{-1} is ascribed to C—H in plane bending frequency of alkanes. The weak band observed at 1051cm^{-1} is attributed to the C—O stretching vibration of carboxylic groups [39].

The FT–IR spectrum of the DTX and FA are shown in Fig. 6(a–c) and the peaks observed at 3500–2850 cm^{-1} (OH and C—H stretching vibration of alkanes), 1674 cm^{-1} (N—H bending vibration), 1379 cm^{-1} (C—H bending vibration, CH_2 and CH_3), 1055 cm^{-1} (C—O—C stretching vibration) and 600–900 cm^{-1} (N—H wagging frequency) [41]. Fig. 6 (a) (d) depicts the AuNPs based conjugates and their peaks presented at 3306–2913 cm^{-1} (OH and C—H stretching vibration of alkanes), 1680–1714 cm^{-1} (N—H bending vibration), 1385 cm^{-1} (C—H bending vibration, CH_2 and CH_3), 1050–1060 cm^{-1} (C—O—C stretching vibration) and 600–900 cm^{-1} (N—H wagging frequency). These peaks confirm that the Dtx and FA particles have successfully bound with AuNPs. These spectra confirm the AuNPs are incorporated with Dtx and FA and formed as conjugates.

3.4. Optical properties of gold based conjugates

Optical properties of the synthesized AuNPs and their corresponding conjugates were confirmed by UV–vis spectroscopy. The UV–vis spectrum of AuNPs is shown in Fig. 6 (b) (a). It shows the SPR absorption peak at 526 nm due to the formation of the spherical shape of nanoparticles [42]. Fig. 6 (b) (b) shows the UV–vis spectra of DTX with at 233 and 288 nm which corresponds to the π–π* transition of the carbonyl group present in the ring [43]. Fig. 6 (b) (c) depicts the UV–vis spectra of FA which was observed peaks at 232 and 344 nm corresponding to the π–π* transitions of aromatic amino groups and amide [44]. AuNPs/DTX/FA conjugates had peaks at 232, 288, 344, and

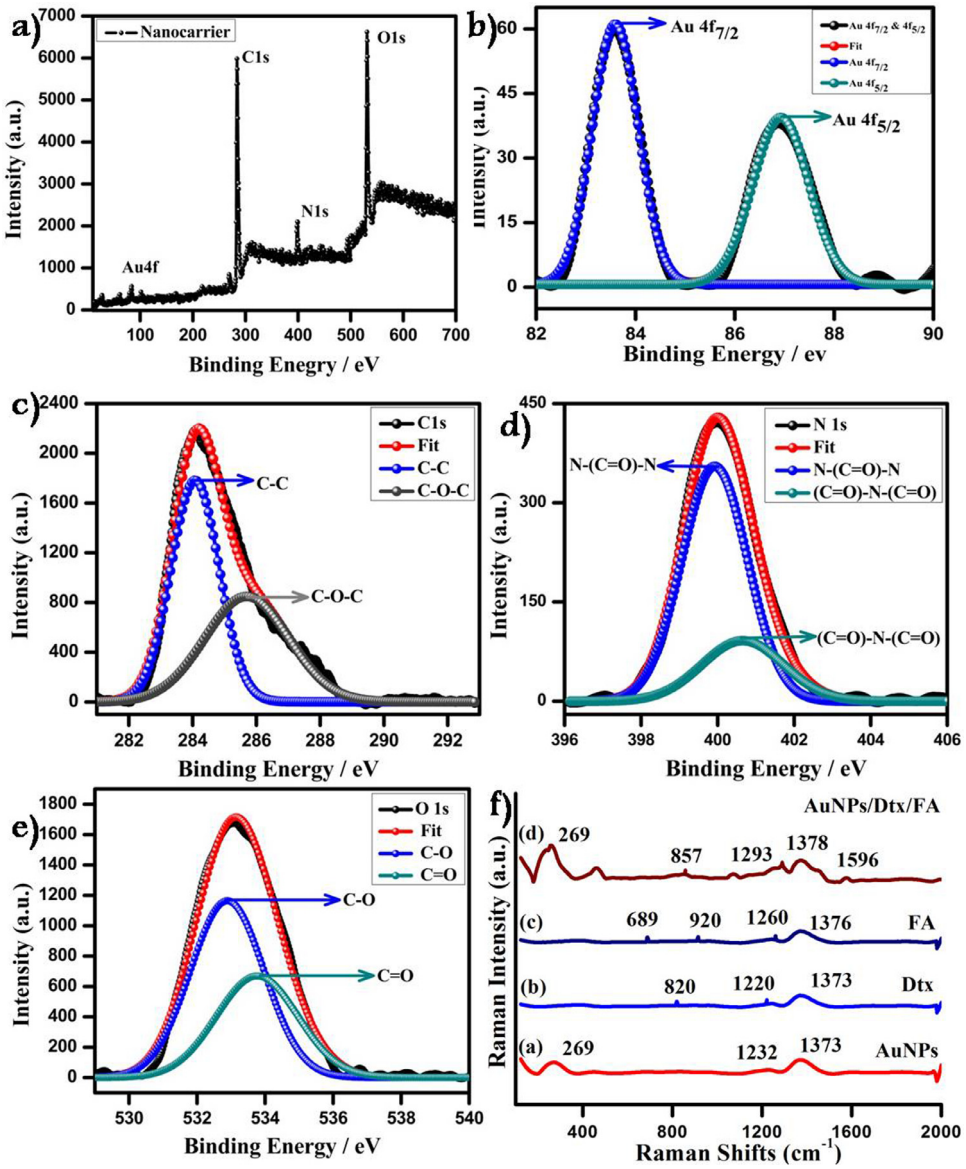

Fig. 5. XPS spectra of AuNPs based nanoconjugates; (a) survey spectrum of AuNPs/Dtx/FA, the high resolution spectrum of gold (b), carbon (c), nitrogen (d) and oxygen (e), respectively. (f) Raman spectra of AuNPs/Dtx/FA nanoconjugates with (a) AuNPs, (b) Dtx, (c) FA and (d) AuNPs/Dtx/FA.

530 nm, corresponding to the formation of the AuNPs based conjugates (Fig. 6 (b) (d)). These spectra clearly indicate the conjugates are clearly attached with the AuNPs which could be used for targeted drug delivery applications.

3.5. In-vitro cytotoxicity study

In order to study the anticancer activity of AuNPs, Dtx, FA and AuNPs based nanoconjugates on proliferation, the H520 lung cancer

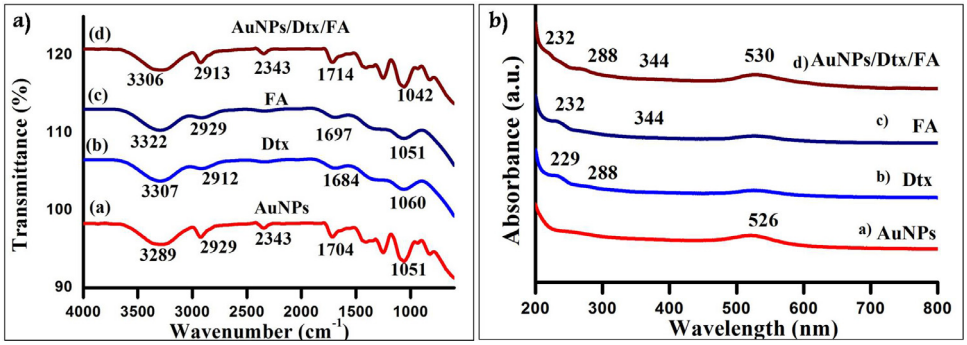

Fig. 6. (a) FT–IR spectra of AuNPs/Dtx/FA based conjugates, (a) AuNPs, (b) Dtx, (c) FA and (d) AuNPs/Dtx/FA conjugates and (b) UV–vis spectra of AuNPs/Dtx/FA nanoconjugates, (a) AuNPs, (b) Dtx, (c) FA and (d) AuNPs/Dtx/FA.

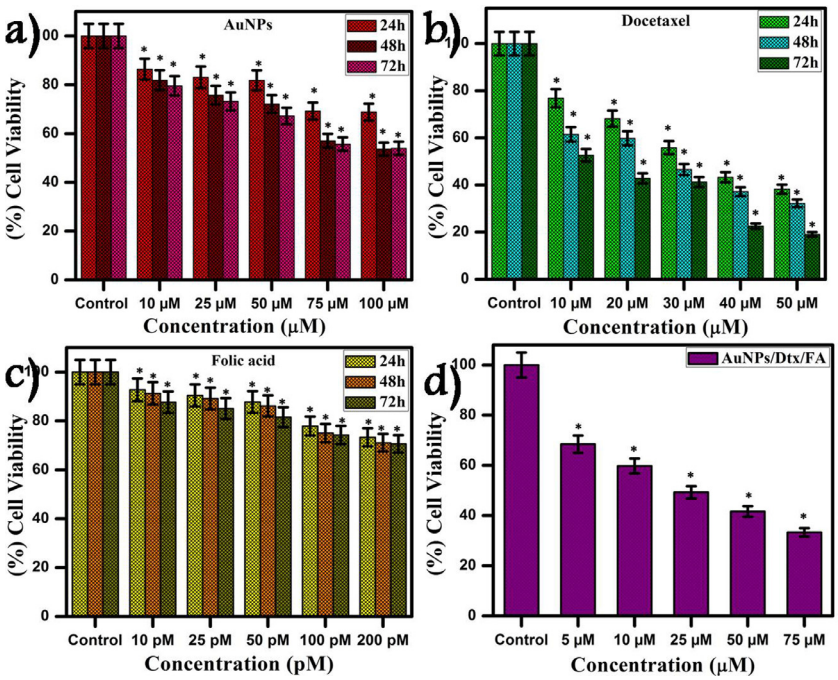

Fig. 7. Cytotoxicity analysis of the AuNPs based nanoconjugates (a) AuNPs, (b) Dtx, (c) FA and (d) AuNPs based nanoconjugates against lung cancer (H520) cell line at 24 h, 48 h and 72 h of post treatment H520 cells. Docetaxel (38 μM) showed good cytotoxicity compared to AuNPs (100 μM) and FA (50 pM) and the nanoconjugates were observed the IC_{50} of 25 μM. (notes: * corresponds to the statistical significance values ($p < 0.05$).

cell line was used (Fig. 7). The cytotoxic effect of AuNPs (a), Dtx (b), FA (c) and (d) nanoconjugates at different concentrations (10 μM, 25 μM, 50 μM, 75 μM, and 100 μM of AuNPs, 10 μM, 20 μM, 30 μM, 40 μM and 50 μM of Dtx and 5pM, 10pM, 25pM, 50pM, 100pM, 200pM and 300pM of FA) and at three different time intervals (24, 48 and 72 h) was analysed using H520 lung cancer cell line. The IC_{50} value of free docetaxel was determined to be 38 μM at 48 h time point. At the same time point, the concentrations for AuNPs and FA were also determined at which we have maximum cell death, thus contributing to an optimum value of AuNPs and FA that can be used in the conjugate development; and to limit cell death to the effect of Dtx alone. We have determined that at the maximum concentration of 100 μM for AuNPs, the cell death was approximately 25% of the control, while FA has almost 100% cell viability in the picomolar concentration. This experiment will help to design better nanoconjugates while knowing the limiting concentrations of the non drug components and decreasing potential non specific targeting.

The combined effect of the AuNPs based nanoconjugates has been evaluated for the cell viability of H520 cell line with unloaded AuNPs/FA and Dtx loaded AuNPs/FA after incubation of 24 h time point. Fig. 7(d) depicts the cytotoxicity of AuNPs/FA/Dtx at micromolar concentration and compare with free AuNPs, Dtx, and FA. The IC_{50} value of docetaxel was observed at 38 μM and this concentration was fixed and the concentration of AuNPs and FA was varied in the medium. From the Fig. 7(d) it can be clearly seen that, with the addition of AuNPs, FA, and Dtx components simultaneously, there is a dramatic decrease in cell survival, almost 50% of control. This result clearly reinforces the fact that Dtx loaded AuNPs/FA is more effective against cancer cell line than free Dtx. Both the dose concentrations and incubation plays a major role in cell toxicity of Dtx.

In particularly, after 24 h incubation, H520 cell viability was decreased to about 75%, 68%, 56%, 47 and 39% for AuNPs/FA/Dtx concentration at 5, 10, 25, 50 and 75 μM, respectively. This results correspond to an increase in the cytotoxicity of 50% ($p < 0.05$) compared with free Dtx.

From the cytotoxicity study, it was observed that synthesized AuNPs based nanoconjugates induced the concentration dependent inhibition against lung cancer cell lines. Some of the approved chemotherapeutic agents provide more side effects and high cost. Hence, there is a need for developing novel alternate medicines for this deadly disease. The results suggest that the synthesized AuNPs based nanoconjugates are a potential nanocarrier for chemotherapeutic agents in the treatment of various cancers.

4. Conclusion

In this study, we have investigated a safe and effective nanocarrier with a focus on targeted drug delivery. The AuNPs were synthesized by chemical reduction method using trisodium citrate under controlled conditions. Optical properties and structural features of the individual nanoparticles and AuNPs/Dtx/FA were studied by UV–vis spectroscopy, Raman and FT–IR spectroscopy. Oxidation state, purity and elemental composition of the AuNPs based nanoconjugates were confirmed by XPS and EDS spectroscopy. The morphological features of the synthesized AuNPs were determined by HR-TEM and FE-SEM analysis, which indicates the particles are spherical shape with highly crystalline in nature (face centered cubic crystal) and have the average dimension of 18 nm. The crystallinity was also confirmed by XRD pattern. The anticancer activities of the AuNPs, Dtx, FA, AuNPs/Dtx, FA/Dtx and, AuNPs/Dtx/FA against lung cancer cell line (H520) were evaluated. The IC_{50} value of docetaxel was observed at 38 μM and this concentration used for the combined effect of AuNPs based nanoconjugates, which showed almost 50% decrease in cell survival compared with control. In conclusion, AuNPs based nanoconjugates can be considered an alternative and promising nanocarrier system to be used for chemotherapeutic agents in the treatment of various cancers.

Acknowledgment

The authors gratefully acknowledge the Department of Biotechnology (DBT), New Delhi for the financial support through the funded project (Targeted drug delivery using gold nanocarrier with special application to prostate cancer: BT/PR3494/NNT/28/561/2011).

Reference

[1] S. Thambiraj, S. Hema, D. Ravi Shankaran, An overview on applications of gold nanoparticle for early diagnosis and targeted drug delivery to prostate cancer, Recent Pat. Nanotechnol. 12 (2) (2018) 110–131.

[2] P.M. Mridula, D.R. Shankaran, Nanoparticle modified drug loaded biodegradable polymeric contact lenses for sustainable ocular drug delivery, Curr. Drug Deliv. 14 (4) (2017) 555–565.
[3] Y. Qian, M. Qiu, Q. Wu, Y. Tain, Y. Zhang, N. Gu, S. Li, L. Xu, R. Li, Enhanced cytotoxic activity of cetuximab in EGRP-positive lung cancer by conjugating with gold nanoparticles, Sci. Rep. 4 (7490) (2014) 1–8.
[4] M.Z. Ahmad, S. Akhter, Z. Rahman, S. Akhter, M. Anwar, N. Mallik, F.J. Ahmad, Nanometric gold in cancer nanotechnology current status and future prospect, J. Pharm. Pharmacol. 65 (2013) 634–651.
[5] S. Hema, S. Thambiraj, D. Ravi Shankaran, Nanoformulations for targeted drug delivery to prostate cancer: an overview, J. Nanosci. Nanotechnol. 18 (8) (2018) 5171–5191.
[6] H.W. Kao, Y.Y. Lin, C.C. Chen, K.H. Chi, D.C. Tien, C.C. Hsia, M.H. Lin, H.E. Wang, Evaluation of EGFR-targeted radioimmuno-gold nanoparticles as a threnostic agent in a tumor animal model, Bioorg. Med. Chem. Lett. 23 (2013) 3180–3185.
[7] M.Y. Lan, Y.B. Hsu, C.H. Hsu, C.Y. Ho, J.C. Lin, S.W. Lee, Induction of apoptosis by high-dose gold nanoparticles in nasopharyngeal carcinoma cells, Auris. Nasus. Larynx. 40 (2013) 563–568.
[8] S.A. Curley, P. Cherukuri, K. Briggs, C.R. Patra, M. Upton, E. Dolson, Mukherjee noninvasive radiofrequency field-induced hyperthermic cytotoxicity in human cancer cells usingcetuximab-targeted gold nanoparticles, J. Exp. Ther. Oncol. 7 (2008) 313–326.
[9] J. Turkevich, P.C. Stevenson, J. Hillier, A study of the nucleation and growth processes in the synthesis of colloidal gold, Discuss Faraday Soc. 11 (1951) 55–75.
[10] G. Frens, Controlled nucleation for the regulation of the particle size in monodisperse gold suspensions, Nat. Phys. Sci. 241 (1973) 20–22.
[11] K. Rahme, J.D. Holmes, Gold Nanoparticles: Synthesis, Characterization, and Bioconjugation, CRC Press, Taylor & Francis, 2015 DOI:/dx.doi.org/10.1081/E-ENN3-120053520.
[12] K. Saha, S.S. Agasti, C. Kim, X. Li, V.M. Rotello, Gold nanoparticles in chemical and biological sensing, Chem. Rev. 112 (5) (2012) 2739–2779.
[13] P. Zhao, D. Astruc, Docetaxel nanotechnology in anticancer therapy, ChemMedChem 7 (6) (2012) 952–972.
[14] L. Gallego-Yerga, I. Posadas, C. de la Torre, J. Ruiz-Almansa, F. Sansone, C.O. Mellet, A. Casnati, J.M.G. Fernández, V. Ceña, Docetaxel-loaded nanoparticles assembled from β-cyclodextrin/calixarene giant surfactants: physicochemical properties and cytotoxic effect in prostate cancer and glioblastoma cells, Front. Pharmacol. 8 (2017) 249.
[15] S. Saito, F. Espinoza-Mercado, H. Liu, N. Sata, X. Cui, H.J. Soukiasian, Current status of research and treatment for non-small cell lung cancer in never-smoking females, Cancer Biol. Ther. 18 (6) (2017) 359–368.
[16] D.P. Petrylak, The treatment of hormone-refractory prostate cancer: docetaxel and beyond, Rev. Urol. 8 (2006) S48–S55.
[17] E. Lee, H. Kim, I.H. Lee, S. Jon, In vivo antitumor effects of chitosan-conjugated docetaxel after oral administration, J. Control Release 140 (2009) 79–85.
[18] H. Zhang, F. Li, J. Yi, C. Gu, L. Fan, Y. Qiao, Y. Tao, C. Cheng, H. Wu, Folate-decorated maleilated pullulan-doxorubicin conjugate for active tumor-targeted drug delivery, Eur. J. Pharm. Sci. 42 (2011) 517–526.
[19] Y. Zhang, J. Li, M. Lang, X. Tang, L. Li, X. Shen, Folate-functionalized nanoparticles for controlled 5-Fluorouracil delivery, J. Colloid. Interface Sci. 354 (2011) 202–209.
[20] C.P. Leamon, J.A. Reddy, I.R. Vlahov, M. Vetzel, N. Parker, J.S. Nicoson, L.C. Xu, E. Westrick, Synthesis and biological evaluation of EC72: a new folate-targeted chemotherapeutic, Bioconjugate Chem. 16 (2005) 803–811.
[21] X. Liang, J. Fan, Y. Zhao, M. Cheng, X. Wang, R. Jin, T. Sun, A targeted drug delivery system based on folic acid-functionalized upconversion luminescent nanoparticles, J. Biomater. Appl. 31 (9) (2017) 1247–1256.
[22] D.R. Shankaran, N. Miura, Recent progress and challenges in nanotechnology for biomedical applications: an insight into the analysis of neurotransmitters, Recent Pat. Nanotechnol. 1 (2007) 210–223.
[23] A.A. Stavrovskaya, Cellular mechanisms of multidrug resistance of tumor cells, Biochemistry 65 (1) (2000) 95–106.
[24] S. Rajkumar, Anticancer activity of eco-friendly gold nanoparticles against lung and liver cancer cells, J. Genet. Eng. Biotechnol. 14 (2016) 195–202.
[25] F.S. Rosarin, V. Arulmozhi, S. Nagarajan, S. Mirunalini, Antiproliferative effect of silver nanoparticles synthesized using amla on Hep2 cell line, Asian Pac. J. Trop. Med. (2012) 1–10.
[26] Z. Liu, Y. Wu, Z. Guo, Y. Liu, Y. Shen, P. Zhou, X. Lu, Effects of internalized gold nanoparticles with respect of cytotoxicity and invasion activity in lung cancer cells, PLoS One 9 (6) (2014) e99175.
[27] M. Uz, V. Bulmus, S.A. Altinkaya, Effect of PEG grafting density and hydrodynamic volume on gold nanoparticle – cell Interactions: an investigation on cell Cycle, Apoptosis, and DNA damage, Langmuir 32 (2016) 5997–6009.
[28] G. Ghodake, D-Y. Kim, J.H. Jo, J. Jang, D.S. Lee, One-step green synthesis of gold nanoparticles using casein hydrolytic peptides and their anti-cancer assessment using the DU145 cell lines, J. Ind. Eng. Chem. (2015) 1–5.
[29] M.R.K. Priya, P.R. Iyer, Anticancer studies of the synthesized gold nanoparticles against MCF 7 breast cancer cell lines, Appl. Nanosci. 5 (4) (2015) 443–448.
[30] R. de Oliveira, P. Zhao, N. Li, L.C. de Santa Maria, J. Vergnaud, J. Ruiz, D. Astruc, G. Barratt, Synthesis and in vitro studies of gold nanoparticles loaded with docetaxel, Int. J. Pharm. 454 (2) (2013) 703–711.
[31] S. Pattanayak, S. Chakraborty, M.R. Mollick, I. Roy, S. Basu, D. Rana, S. Gauri, D. Chattopadhyay, M. Chakraborty, In-situ fluorescence of lac dye stabilized gold nanoparticles; DNA binding assay and toxicity study, New J. Chem. 40 (2016) 7121–7131.
[32] S. Jain, G. Spandana, A.K. Agrawal, V. Kushwah, K. Thanki, Enhanced antitumor efficacy and reduced toxicity of docetaxel loaded estradiol functionalized stealth polymeric nanoparticles, Mol. Pharm. 12 (2015) 3871–3884.
[33] M.F. Cipreste, I. Gonzalez, T.M.M. Martins, A.M. Goes, W.A.A. Macedo, E.M.B. de Sousa, Attaching folic acid on hydroxyapatite nanorods surfaces: an investigation of the HA-FA interaction, RSC Adv. 6 (2016) 76390–76400.
[34] M. Brust, M. Walker, D. Bethell, D.J. Schiffrin, R. Whyman, Synthesis of thiol-derivastised gold nanoparticles in two-phase liquid–liquid system, J. Chem. Soc. Chem. Commun. (1994) 801–802.
[35] J. Tournebize, A. Boudier, A. Sapin-Minet, P. Maincent, P. Leroy, R. Schneider, Role of gold nanoparticles capping density on stability and surface reactivity to design drug delivery platforms, ACS Appl. Mater. Interfaces 4 (2012) 5790–5799.
[36] R.V. Kutty, S. Feng, Cetuximab conjugated vitamin E TPGS micelles for targeted delivery of docetaxel for treatment of triple negative breast cancers, Biomaterials 34 (2013) 10160–10171.
[37] Y. Liua, K. Li, J. Pan, B. Liu, S. Feng, Folic acid conjugated nanoparticles of mixed lipid monolayer shell and biodegradable polymer core for targeted delivery of docetaxel, Biomaterials 31 (2010) 330–338.
[38] R.H. Lahr, P.J. Vikesland, Surface – enhanced Raman spectroscopy (SERS) cellular imaging of intracellulary biosynthesized gold nanoparticles, ACS Sustain. Chem. Eng. 2 (2014) 1599–1608.
[39] P. Cipriani, D. Ben-Amotz, characterization of select members of the taxane family using raman spectroscopy, J. Raman Spectrosc. 36 (2005) 1052–1058.
[40] J.C. John, R. Tomas, E.R. Ciro, B. Anja, Adsorption and vibrational study of folic acid on gold nanopillar structures using surface-enhanced Raman scattering spectroscopy, Nanomater. Nanotechnol. 5 (2015) 29.
[41] H. Kulhari, D. Pooja, S. Shrivastava, S.R. Telukutala, A.K. Barui, C.R. Patra, G.M.N. Vegi, D.J. Adams, R. Sistla, Cyclic-RGDfK peptide conjugated succinoyl-TPGS nanomicelles for targeted delivery of docetaxel to integrin receptor over-expressing angiogenic tumours, Nanomed. Nanotechnol. Biol. Med. 11 (2015) 1511–1520.
[42] Z. Liu, Y. Wu, Z. Guo, Y. Liu, Y. Shen, P. Zhou, X. Lu, Effects of internalized gold nanoparticles with respect of cytotoxicity and invasion activity in lung cancer cells, PLoS One 9 (6) (2014) e99175.
[43] A. FranÅois, A. Laroche, N. Pinaud, L. Salmon, J. Ruiz, J. Robert, D. Astruc, Encapsulation of docetaxel into pegylated gold nanoparticles for vectorization to cancer cells, Chem. Med. Chem. 6 (2011) 2003–2008.
[44] A.K.S. Lafarga, F.P.P. Moisés, A. Gurinov, G.G. Ortiz, G.G.C. Arízaga, Dual responsive dysprosium-doped hydroxyapatite particles and toxicity reduction after functionalization with folic and glucuronic acids, Mater. Sci. Eng. C 48 (2015) 541–547.